AIP | Applied Physics Letters

Amorphous/crystalline silicon interface defects induced by hydrogen plasma treatments

Jonas Geissbühler, Stefaan De Wolf, Bénédicte Demaurex, Johannes P. Seif, Duncan T. L. Alexander et al.

Citation: Appl. Phys. Lett. **102**, 231604 (2013); doi: 10.1063/1.4811253
View online: http://dx.doi.org/10.1063/1.4811253
View Table of Contents: http://apl.aip.org/resource/1/APPLAB/v102/i23
Published by the AIP Publishing LLC.

Amorphous/crystalline silicon interface defects induced by hydrogen plasma treatments

Jonas Geissbühler,[1,a)] Stefaan De Wolf,[1] Bénédicte Demaurex,[1] Johannes P. Seif,[1] Duncan T. L. Alexander,[2] Loris Barraud,[1] and Christophe Ballif[1]
[1]*École Polytechnique Fédérale de Lausanne (EPFL), Institute of Microengineering (IMT), Photovoltaics and Thin-Film Electronics Laboratory, Rue A.-L. Breguet 2, CH-2000 Neuchâtel, Switzerland*
[2]*École Polytechnique Fédérale de Lausanne (EPFL), Interdisciplinary Centre for Electron Microscopy (CIME), Station 12, CH-1015 Lausanne, Switzerland*

(Received 17 May 2013; accepted 27 May 2013; published online 13 June 2013)

Excellent amorphous/crystalline silicon interface passivation is of extreme importance for high-efficiency silicon heterojunction solar cells. This can be obtained by inserting hydrogen-plasma treatments during deposition of the amorphous silicon passivation layers. Prolonged hydrogen-plasmas lead to film etching. We report on the defect creation induced by such treatments: A severe drop in interface-passivation quality is observed when films are etched to a thickness of less than 8 nm. Detailed characterization shows that this decay is due to persistent defects created at the crystalline silicon surface. Pristine interfaces are preserved when the post-etching film thickness exceeds 8 nm, yielding high quality interface passivation. © *2013 AIP Publishing LLC*.
[http://dx.doi.org/10.1063/1.4811253]

Silicon heterojunction (SHJ) solar cells enable high energy conversion efficiencies with industrial processing.[1,2] Intrinsic hydrogenated amorphous silicon (a-Si:H(i)) layers a few nanometers thick are deposited by plasma-enhanced chemical vapor deposition (PECVD) on both sides of a crystalline silicon (c-Si) wafer to reduce the interface-state density.[3] Equally thin doped a-Si:H(p/n) layers are subsequently deposited on either side to create, respectively, the emitter and the back surface field. To enable lateral flow of charge carriers and to efficiently contact the a-Si:H layers, transparent conductive oxide layers are deposited on both sides. Finally, a screen-printed Ag grid and a sputtered Ag layer are deposited on the front and back sides, respectively, as electrical contacts. With this design, efficiencies as high as 24.7% have been reported, with record open-circuit voltages (V_{OC}s) of 750 mV.[1,4]

To obtain high-quality interface passivation, an atomically sharp a-Si:H/c-Si interface is necessary.[5] Additionally, good passivation is obtained for as-deposited films deposited with high SiH_4 depletion,[6] yielding film growth close to the amorphous-to-crystalline silicon transition. Further improvements are obtained by interrupting film deposition and inserting short H_2 plasma treatments of the film growth surface.[7] In this way, the bulk of a-Si:H(i) films can come even closer to the amorphous-to-crystalline transition without risking detrimental epitaxial growth. However, we have observed that such treatments may lead to bandgap widening and the presence of nanosized voids in the a-Si:H. Others have confirmed the beneficial electronic effects that such treatments yield, though without an associated increase in material disorder, using their processing conditions.[8] The influence of H_2 treatments of the c-Si surface *prior to* a-Si:H deposition has also been studied. Such treatments may introduce severe electronic damage of the c-Si surface, which could not be recovered by subsequent a-Si:H passivation.[9,10] Hence, some uncertainty regarding the use of H_2 plasma treatments close to the c-Si surface exists in the literature. On the one hand, such treatments may lead to a-Si:H(i) material that is better for passivation; on the other hand, c-Si surface defects may be induced, dramatically reducing surface passivation.

The effects of *prolonged* H_2 plasma treatments remain unclear as well. A motivation for longer H_2 plasma treatments is to use them for a-Si:H etching (rather than merely for passivation improvement).[11–13] Indeed, advanced device architectures such as SHJ back-contacted solar cells require doped a-Si:H layer patterning, while preserving pristine a-Si:H(i) underlayers for surface passivation and thus the high V_{OC}s typical for SHJ devices.[14–16] A clear advantage of dry etching for the fabrication of SHJ back-contacted solar cells is that both etching and deposition can take place in the same system without vacuum break.

We report in this paper on the effect of H_2 plasma etching on both the bulk a-Si:H properties and the surface passivation quality of the c-Si underneath. We demonstrate that despite modification of the a-Si:H(i) microstructure, good surface passivation can be maintained under the necessary condition that a sufficiently thick (few nanometers) passivation film remains present, shielding the c-Si surface from plasma damage. With this technique, we obtain highly reproducible etch rates. From a device point-of-view, these findings offer great promise for doped a-Si:H layer patterning while maintaining good surface passivation.

Figure 1(a) shows the experimental sequence we followed: (1) High-quality float-zone 4 Ω cm phosphorus-doped double side polished ⟨111⟩ wafers were dipped in diluted hydrofluoric acid solution (HF) for 1 min to remove the native oxide. (2) An a-Si:H(i/n) stack was deposited on the back side to provide the most efficient passivation both by lowering the interface-state density and by providing an additional field effect at this surface. PECVD depositions were carried out directly after the HF dip by using an

a)Author to whom correspondence should be addressed. Electronic mail: jonas.geissbuehler@epfl.ch

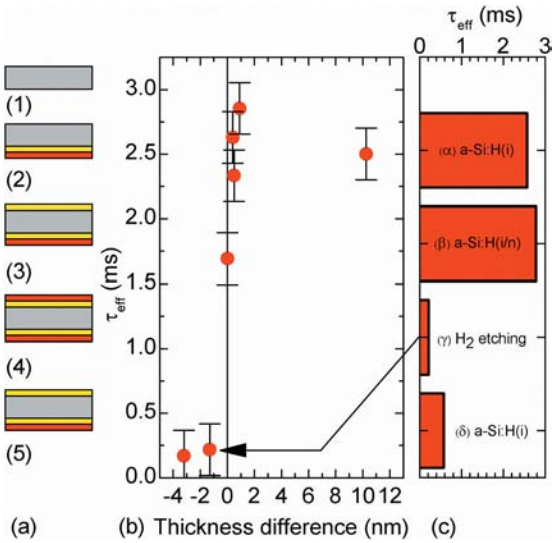

FIG. 1. (a) Experimental sequence: (1) DSP ⟨111⟩ c-Si wafer after the HF dip, (2) a-Si:H(i/n) stack deposited on the back side, (3) a-Si:H(i) deposition on the front side, (4) a-Si:H(n) deposition on the front side, (5) H_2 etching on the front side. (b) Minority-carrier lifetime after the H_2 etching at a carrier injection level of 5×10^{15} cm^{-3} vs. the thickness difference between the H_2-etched (after step 5) and as-deposited a-Si:H(i) layer (after step 3). (c) Minority-carrier lifetime evolution along the entire process for the sample highlighted in (b).

Octopus-I PECVD cluster tool (INDEOtec). Deposition details can be found elsewhere.[17] (3) An 8-nm-thick a-Si:H(i) layer was then deposited on the front side. (4) An 11-nm-thick a-Si:H(n) layer was deposited on the front side. The thickness of the layers is representative to those used in real devices.[17] (5) H_2 plasma etching of the front a-Si:H(n) layer was carried out using the same PECVD reactor with pure hydrogen at 1.5 mBar and a 200 °C substrate temperature; the etching time was varied. The plasma was driven by a radio frequency (13.56 MHz) excitation with ≈100 mW/cm^2 power density. Following steps (3), (4) and (5), the samples were systematically characterized by photoconductance decay[18] (PCD, Sinton Consulting WCT-100) and spectroscopic ellipsometry (SE, Horiba UVISEL^{TM}) to measure, respectively, the minority-carrier lifetime (τ_{eff}) and layer thickness.

With these parameters, we obtain a highly reproducible etch rate of 2.3 ± 0.1 nm/min. We observe an incubation time prior to the start of etching of ≈30 s, possibly due to creation of a hydrogen-rich sub-layer at the a-Si:H surface, during which hydrogen diffusion into the film dominates over etching.[12,13] Figure 1(b) shows τ_{eff} measured after etching as a function of the thickness difference between the H_2-etched (after step 5) and the as-deposited a-Si:H(i) buffer layer (after step 3). Negative values point to partial etching of the underlying a-Si:H(i) buffer layer whereas positive values indicate that a-Si:H(n) is partially remaining on the a-Si:H(i) buffer layer. An abrupt drop in τ_{eff} is observed when the a-Si:H(i) layer starts to be etched (i.e., thickness difference < 0). From this, we conclude that it may be possible to etch the doped layer away fully, which opens possibilities for film patterning, but seemingly we need to preserve the nominal buffer layer thickness to guarantee high-quality passivation.

To further investigate the effect of reduced a-Si:H(i) buffer layer thickness on the passivation quality, a-Si:H(i) re-depositions were carried out following over-etching of the a-Si:H(n) layer, to restore the initial buffer layer thickness. Figure 1(c) shows the evolution of τ_{eff} for the sample highlighted in Fig. 1(b), following the different process steps including re-deposition. Beginning with the sample having only an a-Si:H(i) layer with typical buffer layer thickness (α), a τ_{eff} increase is observed with a-Si:H(n) deposition, most likely induced by additional field-effect passivation (β). Next, τ_{eff} drops severely from 2.8 ms to 200 μs due to H_2 etching (γ). This drop is not recovered by re-deposition of a-Si:H(i) (δ). From this, we conclude that the passivation losses are linked to defect formation (either at the c-Si surface, or in the remaining film) rather than merely from the reduction of the passivation layer thickness.

To decouple the contribution of c-Si surface defects from a-Si:H modification, etching of the *full* a-Si:H(i/n) stack was carried out. In this case, the plasma duration was set to precisely etch the complete a-Si:H(i/n) stack without over-etching, thus keeping the c-Si wafer pristine. To prevent native oxide formation following the etching, subsequent re-deposition of an a-Si:H(i) passivation layer was carried out without vacuum break. In this case, τ_{eff} decreased from 1.3 ms for the a-Si:H(i/n) precursor to 290 μs despite the re-deposition of a buffer layer (data not shown).

High-resolution transmission electron microscopy (HR-TEM, Philips CM300 UT) was used to inspect the a-Si:H/c-Si interface following the described experiments. Cross-section samples were prepared using mechanical polishing (Allied High Tech Multiprep) followed by low-energy Ar ion milling. Figure 2(a) shows a HR-TEM image of the c-Si surface with an as-deposited a-Si:H(i/n) stack. We observe

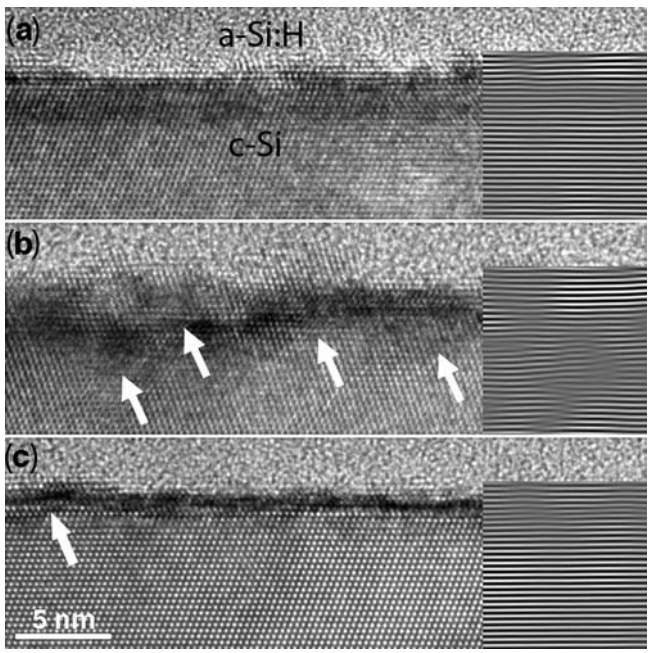

FIG. 2. HR-TEM micrographs of the c-Si/a-Si:H interface for (a) an as-deposited a-Si:H(i/n) stack, (b) a completely etched a-Si:H(i/n) stack followed by a re-deposited a-Si:H(i) layer, and (c) an a-Si:H(i/n) stack after selective etching of the a-Si:H(n) layer. The right side of each image is treated with a Fourier filtering, highlighting the (110) crystalline plane.

an atomically sharp a-Si:H/c-Si transition, as is required to obtain high-quality surface passivation.[5] The darker area at the interface may be due to image delocalization or slight lattice imperfections in the first few nanometers of the substrate. A c-Si surface roughness lower than 2 nm is observed, which may indicate imperfect wafer mirror polishing or HF-dip-related wafer etching. Figure 2(b) shows the sample described earlier for which the entire a-Si:H(i/n) stack was etched and followed by a subsequent a-Si:H(i) re-deposition. We observe clearly an increase in the c-Si surface roughness to ≈5 nm and the appearance of defects in the near-surface crystalline structure (indicated by white arrows). Indeed, with Fourier filtering, defects and distortions are observed in the c-Si lattice as deep as 10–15 nm beneath the wafer surface (see insets). Figure 2(c) shows the a-Si:H/c-Si interface for a sample for which only the a-Si:H(n) layer was etched while preserving the full a-Si:H(i) buffer layer. This is the sample with a zero thickness difference shown in Fig. 1(b). Contrary to the case of full-stack etching, the initial low c-Si surface roughness and low defect density in the crystalline structure are preserved. This set of images confirms that severe microstructural damage of the c-Si surface occurs when the H_2 plasma starts to interact with this interface.[19] This effect is avoided by leaving the full a-Si:H(i) buffer layer un-etched. According to the steep drop in τ_{eff} observed in Fig. 1(b), about 8 nm of a-Si:H(i) is required to provide sufficient shielding of the c-Si surface to avoid irreversible sub-surface defect creation. Despite this, some minor defects seem to be present at the interface in Fig. 2(c); hence, it may be asked to what extent the microstructure of the remaining a-Si:H(i) buffer layer is modified during etching of the a-Si:H(n) overlayer.

To answer this question, attenuated total reflectance (ATR) Fourier transform infrared (FTIR) and SE were used to probe the a-Si:H(i) microstructural modifications. The a-Si:H ATR-FTIR absorbance spectra are largely governed by the silicon-hydrogen bonding environment. Information about the precise Si–H bonding environment can be deduced from the high and low stretching mode (HSM, LSM) absorption peaks at 2070–2100 cm^{-1} and 1980–2010 cm^{-1}, respectively.[20] The LSM is assigned to the monohydride bonding configuration, whereas the HSM is a signature of (hydrogenated) nanometric voids in the bulk material.[21] Four c-Si prisms were processed separately and characterized with ATR-FTIR and SE to assess the a-Si:H material properties after each process step.[22] The deposition parameters were identical to those in the experiments described earlier. The a-Si:H(n) layer was replaced by an a-Si:H(i) layer (labeled i2) to avoid free-carrier absorption artifacts during FTIR characterization. We label the original a-Si:H(i) buffer layer as i1. Sample (1) is a 15-nm-thick as-deposited a-Si:H(i) reference layer. Sample (3) was prepared as sample (1), and immediately followed by a H_2 etching step of the duration needed (3.48 min here) to completely remove the i2 layer without etching any i1 material. Sample (4) features an additional a-Si:H(i) re-deposition step (labeled i3) after H_2 etching to restore the initial 15 nm thickness. For as-deposited a-Si:H, the Si–H bonding environment is known to vary across the thickness of thin films.[23] Therefore, ATR-FTIR spectrum comparisons must be made between samples of similar thickness. For this purpose, sample (2) contains 7 nm of as-deposited a-Si:H(i) to provide a reliable comparison with sample (3). Sample thickness measured by SE is displayed in Fig. 3(c). Figure 3(a) shows the ATR-FTIR absorbance spectra of the four samples. The HSM/LSM peak deconvolution is displayed for sample (1). A usual figure of merit in infrared spectroscopy of a-Si:H is the microstructure factor R*, defined as the ratio of the integrated HSM and LSM peaks after deconvolution.[24] Figure 3(b) shows R* for the four samples. By comparing the spectra of samples (2) and (3), we note a clear increase of the HSM peak (increase of R*) after H_2 etching, which points at more void-rich material. A similar comparison can be made between samples (1) and (4) though the re-deposition of the as-deposited i3 layer reduces the magnitude of this effect. A clear increase of the HSM can be seen for sample (4), indicating a higher void-related hydrogen content in the layer. A bandgap widening observed between sample (1) and (4) from 1.86 eV to 1.94 eV confirms such hydrogen incorporation.[7,8,25]

To study the source of hydrogen present in the films *after* etching, H_2/D_2 etching experiments followed by thermal desorption spectroscopy (TDS) were done. H_2/D_2 effusion rate profiles are characterized by high and low temperature peaks, qualitatively corresponding, respectively, to monohydride and dihydride bond breaking. Further details can be found elsewhere.[26] In addition, the TDS quadrupole mass spectrometer allows for discrimination between H_2 and D_2 species.[27] Therefore, if etching is carried out with D_2 instead of H_2, the HD or D_2 effusion rate profiles will be a signature of atoms incorporated into the film during etching.

Several c-Si samples were prepared with on both sides films featuring a sequence consisting of six deposition/etching steps as shown in Fig. 4(a). Depositions were carried out with SiH_4 diluted in H_2 and etching was done either with H_2

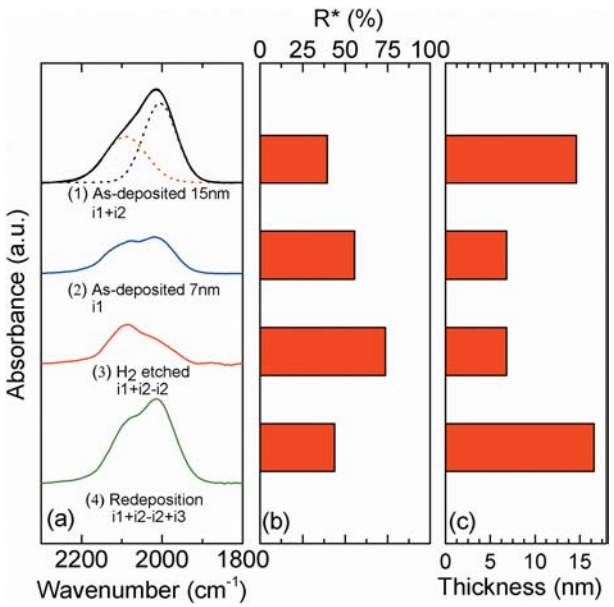

FIG. 3. (a) ATR-FTIR spectra for (1) 15-nm-thick as-deposited a-Si:H(i) (i1 + i2), (2) 7-nm-thick as-deposited a-Si:H(i) (i1), (3) H_2-etched a-Si:H(i) (i1 + i2 − i2), and (4) 15-nm-thick H_2-etched and re-deposited a-Si:H(i) (i1 + i2 − i2 + i3). The deconvolution into the HSM/LSM peaks is shown for sample (1). (b) Microstructure factor extracted from the LSM and HSM deconvolutions. (c) a-Si:H(i) layer thickness measured by SE.

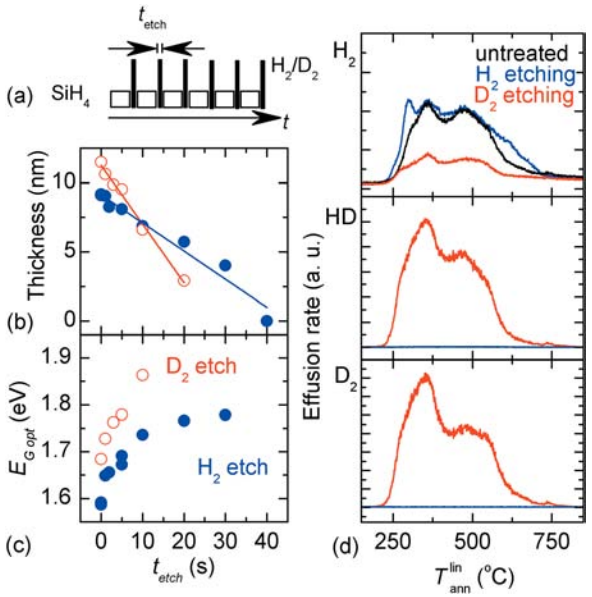

FIG. 4. (a) Deposition/etching sequence. (b) Thickness measured by SE as a function of the duration of each plasma etching step. (c) Optical bandgap as a function of the duration of each plasma etching step. (d) H_2, HD, and D_2 effusion rate profiles as a function of sample temperature. H_2 etched samples were previously presented in Ref. 7.

or with D_2 using parameters similar to those described earlier. The deposition time was kept constant whereas the duration of the H_2/D_2 etching step varied from 0 to 40 s. Therefore, the cumulative duration of the plasma etching varied from 0 to 4 min. The samples were characterized by SE and TDS. Figure 4(b) shows the layer thickness measured by SE. A 2.0 nm/min H_2 etch rate was deduced by linear fitting. This lower value compared to the 2.3 nm/min etch rate previously mentioned we explain by the etching incubation time occurring in this case at the beginning of each etching step. A 4.2 nm/min D_2 etch rate was measured. Given the H_2/D_2 mass ratio, this increased etch-rate ratio suggests a physical sputtering mechanism enhanced by the higher momentum of D atoms impinging on the surface. These results confirm earlier findings.[28] Figure 4(c) shows the optical bandgap as a function of the duration of the plasma etching. As mentioned earlier, H_2 etching induces a bandgap widening; apparently, D_2 etching enhances this widening. Figure 4(d) shows the H_2, HD, and D_2 effusion rate profiles of unetched, H_2-etched, and D_2-etched samples with identical film thickness. By comparing the pristine sample with its H_2-etched counterpart, we observe additional H_2 incorporation induced by H_2 etching. This explains the optical bandgap widening. Interestingly, the H_2 effusion rate dramatically drops for the D_2-etched sample, but the HD and D_2 effusion rates indicate that a significant quantity of deuterium is incorporated into the a-Si:H, both as mono- and dihydride. Therefore, this experiment demonstrates that a significant exchange of hydrogen between film and etch plasma occurs during etching, pointing also at film mixing during such a procedure.

Our findings are thus as follows: Hydrogen plasmas can be used to accurately etch a-Si:H films for patterning purposes. To guarantee an electronically pristine c-Si surface, at least a few nanometers of a-Si:H should remain on the surface to avoid irreversible damage. The remaining film is subject to significant microstructural changes, where exchanges of hydrogen may take place and the film bandgap widens due to hydrogen incorporation. These changes have no detrimental effect on the interface passivation quality. Since the minimum layer thickness needed to provide an efficient shielding of the c-Si surface from the H_2 etch plasma corresponds precisely with the a-Si:H(i) buffer layer thickness used for silicon heterojunction solar cells, such etching opens possibilities for doped a-Si:H layer patterning and could be used, e.g., for the development of advanced device architectures such as back-contacted solar cells with heterostructure contacts.

The authors gratefully acknowledge Jakub Holovsky for ATR-FTIR measurements as well as Aïcha Hessler-Wyser, Antoine Descoeudres, and Zachary Holman for fruitful discussions, and Colette Vallotton and Danièle Laub of CIME for HR-TEM sample preparation. This work was supported by the European Community's FP7 Program under the 20plμs Project (Grant Agreement No. 256695), the Swiss Commission for Technology and Innovation, the Swiss Federal Energy Office and Axpo Naturstrom Fonds Switzerland. Bénédicte Demaurex and Johannes Seif also acknowledge EuroTech Universities Alliance for financial support.

[1]T. Kinoshita, D. Fujishima, A. Yano, A. Ogane, S. Tohoda, K. Matsuyama, Y. Nakamura, N. Tokuoka, H. Kanno, H. Sakata, M. Taguchi, and E. Maruyama, in *Proceedings of the 26th European Photovoltaic Solar Energy Conference and Exhibition* (WIP, Hamburg, Germany, 2011), p. 871.
[2]S. De Wolf, A. Descoeudres, Z. C. Holman, and C. Ballif, Green **2**, 7 (2012).
[3]M. Tanaka, M. Taguchi, T. Matsuyama, T. Sawada, S. Tsuda, S. Nakano, H. Hanafusa, and Y. Kuwano, Jpn. J. Appl. Phys., Part 1 **31**, 3518–3522 (1992).
[4]M. Taguchi, A. Yano, S. Tohoda, and K. Matsuyama, in *Proceedings of the 39th IEEE Photovoltaic Specialists Conference*, Tampa, FL, USA, 2013.
[5]S. De Wolf and M. Kondo, Appl. Phys. Lett. **90**, 042111 (2007).
[6]A. Descoeudres, L. Barraud, R. Bartlome, G. Choong, S. De Wolf, F. Zicarelli, and C. Ballif, Appl. Phys. Lett. **97**, 183505 (2010).
[7]A. Descoeudres, L. Barraud, S. De Wolf, B. Strahm, D. Lachenal, C. Guerin, Z. C. Holman, F. Zicarelli, B. Demaurex, J. Seif, J. Holovsky, and C. Ballif, Appl. Phys. Lett. **99**, 123506 (2011).
[8]M. Mews, T. F. Schulze, N. Mingirulli, and L. Korte, Appl. Phys. Lett. **102**, 122106 (2013).
[9]S. N. Granata, T. Bearda, F. Dross, I. Gordon, J. Poortmans, and R. Mertens, Energy Procedia **27**, 412–418 (2012).
[10]J. W. A. Schüttauf, C. H. M. van der Werf, W. G. J. H. M. van Sark, J. K. Rath, and R. E. I. Schropp, Thin Solid Films **519**, 4476–4478 (2011).
[11]R. C. van Oort, M. J. Geerts, J. C. van den Heuvel, and J. W. Metselaar, Electron. Lett. **23**, 967–968 (1987).
[12]F. Kaïl, A. Fontcuberta, I. Morral, A. Hadjadj, P. Roca, I. Cabarrocas, and A. Beorchia, Philos. Mag. **84**(6), 595–609 (2004).
[13]A. Fontcuberta i Morral and P. Roca i Cabarrocas, J. Non-Cryst. Solids **299–302**, 196–200 (2002).
[14]R. J. Schwartz and M. D. Lammert, in *Proceedings of the IEEE International Electron Devices Meeting* (Washington, DC, 1975), Vol. 21, pp. 350–352.
[15]N. Mingirulli, J. Haschke, R. Gogolin, R. Ferré, T. F. Schulze, J. Düsterhöft, N.-P. Harder, L. Korte, R. Brendel, and B. Rech, Phys. Status Solidi (RRL) **5**, 159–161 (2011).
[16]S. M. Greil, N. Mingirulli, L. Korte, K. Hartmann, A. Schöpke, J. Rappich, and B. Rech, Energy Procedia **8**, 269–274 (2011).
[17]A. Descoeudres, Z. C. Holman, L. Barraud, S. Morel, S. De Wolf, and C. Ballif, IEEE J. Photovoltaics **3**, 83–89 (2013).
[18]R. A. Sinton and A. Cuevas, Appl. Phys. Lett. **69**, 2510 (1996).
[19]M. Shinohara, T. Kuwano, Y. Akama, Y. Kimura, M. Niwano, H. Ishida, and R. Hatakeyama, J. Vac. Sci. Technol. A **21**, 25 (2003).

[20]J. C. Knights, G. Lucovsky, and R. J. Nemanich, J. Non-Cryst. Solids **32**, 393–403 (1979).
[21]A. H. M. Smets, W. M. M. Kessels, and M. C. M. van de Sanden, Appl. Phys. Lett. **82**, 1547 (2003).
[22]B. Demaurex, S. De Wolf, A. Descoeudres, Z. C. Holman, and C. Ballif, Appl. Phys. Lett. **101**, 171604 (2012).
[23]H. Fujiwara and M. Kondo, Appl. Phys. Lett. **86**, 032112 (2005).
[24]J. Müllerová, P. Šutta, G. van Elzakker, M. Zeman, and M. Mikula, Appl. Surf. Sci. **254**, 3690–3695 (2008).
[25]T. F. Schulze, L. Korte, F. Ruske, and B. Rech, Phys. Rev. B **83**, 165314 (2011).
[26]S. De Wolf and M. Kondo, Appl. Phys. Lett. **91**, 112109 (2007).
[27]W. Beyer, Physica B **170**, 105–114 (1991).
[28]H. Iwakuro, T. Kuroda, D. H. Shen, and Z. Lin, J. Vac. Sci. Technol. B **14**, 707 (1996).